This is related to Eq. (11) for δr by the following relations:

$$\epsilon p_M = -\left(\frac{na^2}{2}\right)\frac{\delta a}{a}$$

$$\epsilon p_{\epsilon_l} = \frac{\delta M}{n} + \frac{ah}{\mu e}\hat{b}\cdot\delta e$$

$$\epsilon p_h = \frac{h\times\delta h}{h^2} \equiv \delta\theta_\perp$$

$$\epsilon P_e = \frac{\mu a}{h^2} h\times\delta e$$

It follows that

$$\frac{\epsilon}{\mu}[h\times P_e + (P_e\times v)\times r] = -a\delta e\left(\hat{e} + \frac{\mu e}{h^2} r\cdot\hat{b}\hat{b}\right)$$

$$+\delta\theta_\parallel \times r - \frac{ah}{\mu e}(\hat{b}\cdot\delta e)v$$

where $\delta\theta_\parallel = \delta\theta - \delta\theta_\perp = \hat{h}e^{-1}\hat{b}\cdot\delta e$.

Marec's Eq. (A1) has the drawback of involving constants that are not entirely independent of one another or subject to direct geometrical interpretation. There is some advantage, therefore, to using Eq. (11) instead.

References

[1] Battin, R.H., *Astronomical Guidance,* McGraw-Hill Book Co., New York, 1964.

[2] Marec, J.P., *Optimal Space Trajectories,* Elsevier, New York, 1969.

[3] Pines, S. and T.C. Fang, "A Uniform Closed Solution of the Variational Equations for Optimal Trajectories During Coast," *Advanced Problems and Methods for Space Flight Optimization,* edited by B. de Venbeke, Pergamon Press, New York, 1969.

[4] Jones, J.B., "A Solution of the Variational Equations for Elliptic Orbits in Rotating Coordinates," AIAA Paper 80-1690, 1980.

AIAA 82-4256

Optical Measurements and Attitude Motion of HERMES After Loss of Stabilization

F.R. Vigneron*
Department of Communications, Ottawa, Canada
and
W.E. Krag†
Massachusetts Institute of Technology, Lexington, Mass.

Introduction

THE three-axis stabilized HERMES communications satellite relied on the gyroscopic stiffness of a momentum wheel for roll and yaw stability. The satellite and its control system are described in Ref. 1, and its configuration is shown in Fig. 1. The basis for stability is essentially the dual-spin principle with a minimum moment of inertia configuration, the central body and solar sails being the "platform" and the momentum wheel the "rotor." If the wheel despins, a loss of attitude stability results.

On day 329 of 1979, an Earth sensor malfunctioned and, in conjunction with degraded telemetry and batteries the wheel despun, resulting in loss of attitude stability and ultimately shutdown of the satellite. The satellite also lost its rf transmit and receive capability shortly after the malfunction. From day 331 of 1979 to mid-1980, the sun's reflections from HERMES were periodically recorded at the Ground-Based Electro Optical Deep Space Surveillance (GEODSS) experimental test site (ETS) in New Mexico.[2] During this time, HERMES made a transition from the unstable state to a flat spin about the yaw axis, and its flat spin decayed to zero.

This Note describes the ETS observations, the correlation with theoretical knowledge, and the deduced attitude motion.

Sequence of the Attitude Motions

Immediately following the malfunction, the onboard controller went to a failure-protect mode which held wheel speed constant. A roll-yaw nutation cone of about 20 deg and a slow pitch rotation (3.1×10^{-3} rad/s) were then induced by thrusters. Within 15 min, the solar array was unable to track the sun, resulting in a battery drain. The batteries were degraded after nearly 4 yr of operation, and provided momentum wheel operation for only a few hours. Thereafter, the wheel lost drive power. The following phases of attitude motion then evolved. The pitch, roll, and yaw axes are the minimum, intermediate, and maximum moment of inertia axes, respectively, and the corresponding moments of inertia are 72, 833, and 858 slug-ft^2.

Despin of the Momentum Wheel

After loss of power, the wheel despun within about 30 min. Its stored momentum (about 16.8 ft-lb-s) transferred to the satellite body, causing a substantial rotation about pitch (about 0.238 rad/s). Numerical simulation indicates that the 20-deg nutation stayed constant during wheel despin.

Change from Spin About Pitch to Spin About Yaw

Energy sink theory applies for this phase. The dynamic state at the outset (spin about pitch with a 20-deg nutation) is near the maximum energy state. The minimum energy state is pure (flat) spin about yaw. The dissipative forces which induce the satellite toward its minimum energy state are

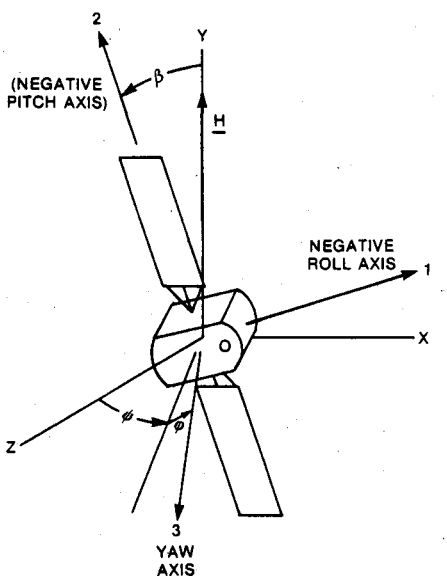

Fig. 1 The HERMES configuration and coordinates. *OXYZ* are inertially fixed. The momentum wheel axis is parallel to the pitch axis. Each of the two solar sails consists of a thin kapton blanket covered with solar cells, and a supporting silver-plated boom.

Received April 14, 1981; revision received May 7, 1982.

*Research Scientist. Member AIAA.

†Staff Member, Lincoln Laboratory.

structural damping of the solar array, and fluid motions of a liquid mercury nutation damper, a heat pipe, and a bladder-pressurized hydrazine system. Reference 3 describes the energy sink method, and extends it to include β-$\dot{\beta}$ phase planes (β is shown in Fig. 1) and results associated with unequal transverse moments of inertia. Two subphases are identified. In the first, the motion consists of rotation about pitch together with coning about the angular momentum vector. β is essentially constant for long periods of time, and slowly increases as the energy level decreases. ψ changes slowly and is periodic (period P_ψ). The period of pitch rotation, P_ω, is short. The two characteristic periods are:

$$P_\omega = 2\pi B/(H\cos\beta) \quad (1)$$

$$P_\psi = 2\pi C/H \quad (2)$$

In the second subphase, the motion is a rotation about yaw with period P_ψ, together with an oscillatory motion about pitch. The oscillation is a degraded state of the earlier pitch rotation which "captured" because of the unequal transverse moments of inertia. The oscillation is dependent on the energy level and tends toward zero as the minimum energy state is approached. The β-$\dot{\beta}$ phase planes show that the transition from the first to second subphases occurs when β is 87.2 deg and that 99% of the dissipative energy is associated with the first subphase.

The Euler equations for the satellite were solved together with damper and kinematic equations, and graphics software was used to display the motion on a CRT. The animation enabled a viewer to develop a feeling for the transition very quickly, and to identify the important satellite surfaces and attitude motion periods that were relevant to the GEODSS observations.

A 31-in. aperture tracking telescope on an equatorial mount was used to track the satellite. The satellite's brightness was measured directly from the video signal from an intensified Ebsicon video camera on the telescope. The video signal was integrated and recorded on a strip chart at the standard TV rate of 30 samples per second. The satellite brightness was displayed on a television monitor, and was measured by comparison with calibration stars in the vicinity. During the first subphase, solar reflections from the back and front of solar array and the north or south radiator panels were observed, and periods P_ψ and P_ω were determined. β vs time, as shown in Fig. 2, was established from the measurements and Eq. (1), and shows that the transition to flat spin occurred over about 15 days. The second subphase was also observed, and the decay of oscillation lasted between 1 and 3 days.

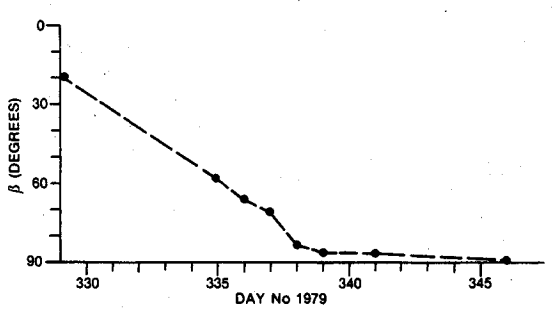

Fig. 2 β vs day number, as calculated by optical measurements of the short period and Eq. (1).

Flat Spin and Despin

Figure 3 shows data taken when HERMES was in a state of pure (flat) spin about yaw. The large variable (from 13th to 10th magnitude) reflections have a stable period beginning at 292 s and increasing slowly with time. Both pieces of data show a characteristic double peak. An orientation where the spin axis lies in the Earth's equatorial plane, perpendicular to the line of sight to the satellite, with the solar panels tilted with respect to the plane of rotation, agrees well with the observed signature of Fig. 3. The large double peak is due to reflections from the silver-plated booms of the solar array, and the broader peaks are due to the cell side of the solar panels or some other diffuse surface on the satellite body. The observed rate of flat spin vs time is presented in Fig. 4. There is no reliable theoretical model to predict the spin rate, due to the absence of flight experience with the particular configuration and orbit. The observed despin is probably due to solar pressure acting on the two solar sails that are believed to be rotated relative to each other. A relative rotation of 2.5 deg would cause a propellor torque sufficient to induce the observed despin.

Double Peak and Array Deformation

The double peaks of Fig. 3 are specular reflections from the two 23 ft long, 1 3/8 in. diam silver-plated booms of the solar array. The peaks are doublets because the two booms are separated by the central body, are not quite in line, and are curved due to bending stresses. The timing of the peaks indicate that the relative misalignment angle is about 3.5 deg. This number agrees with corresponding ones derived through analysis of solar torque measurements made before the malfunction.

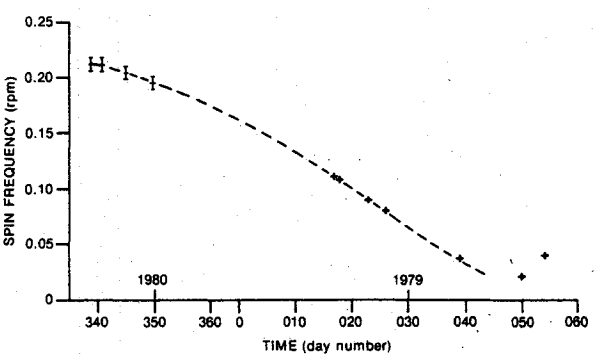

Fig. 4 A plot of the "flat spin" frequency as a function of time. The spin frequency is the inverse of the time between successive appearances of the double peaks shown in Fig. 3.

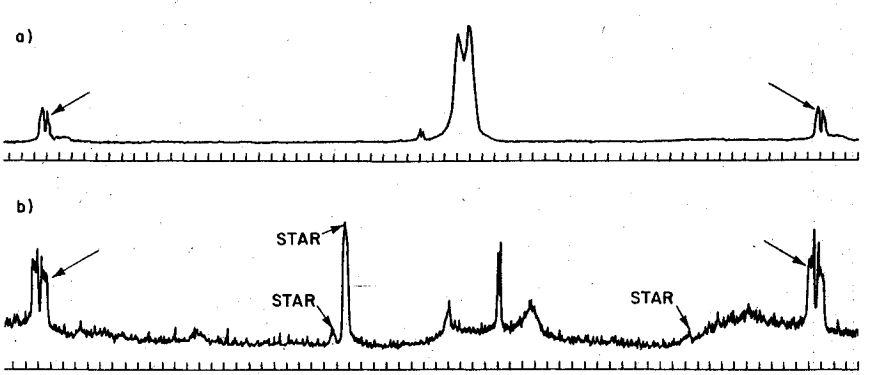

Fig. 3 Brightness variation of HERMES on day 350: a) at 500 GMT, b) at 0800 GMT. For both curves, time increases to the left, and the time scale is 5 s/division. Increased brightness is to the top of the figure. The separation of the double peaks (indicated by arrows) measures the rotation period of the satellite. The double peaks were approximately constant in intensity from day 339 of 1979 to day 52 of 1980. The signature structure near the center changes in relative position as well as intensity.

Acknowledgments

Part of the work reported in this paper was performed with the support of the Department of the Air Force at Lincoln Laboratory. The views and conclusions contained in this document should not be interpreted as necessarily representing the official policies, either expressed or implied, of the U.S. Government.

References

[1] Vigneron, F.R. and Millar, R.A., "Flight Performance of the Stabilization System of the Communications Technology Satellite," *Journal of Guidance and Control,* Vol. 1, Nov.-Dec. 1978, pp. 404-412.

[2] Weber, R., "The Passive, Ground-Based, Electro-Optical Detection of Synchronous Satellites," TN-1978-27, ESD-TR-78-213, MIT Lincoln Laboratory, Lexington, Mass., June 1978.

[3] Vigneron, F.R. and Krag, W.E., "The Attitude Dynamics of Hermes After Termination of Three-Axis Stabilization," CRC Report No. 1354, Dept. of Communications, Ottawa, Canada, 1982.

AIAA 82-4257

Discrete-Time Stability of Continuous-Time Controller Designs for Large Space Structures

Mark J. Balas*
Rensselaer Polytechnic Institute, Troy, N.Y.

I. Introduction

In most of the stable control designs for flexible structures, continuous time is assumed. Yet, it is well known that the controller will be implemented by one or more on-line digital computers; hence the discrete-time stability of such controllers is an important consideration.

For example, it is known the direct-velocity feedback (DVFB), i.e., negative feedback from collocated force actuators and velocity sensors, is a purely dissipative control law and hence cannot produce residual mode instabilities when it is designed for a reduced-order model of a structure.[1-3] However, the stability results are only known for continuous time; it is not immediately clear how much delay due to digital implementation of DVFB can be tolerated without loss of stability. In this Note, we will present some new results which answer this question in the sense that bounds on the time-step size will be given.

The class of distributed parameter systems, which includes flexible structures, may be described by the following:

$$v_t = Av + Bf \qquad v(0) = v_0 \qquad y = Cv \tag{1}$$

where, for each positive time t, the (possibly vector-valued) system state $v(t)$ is in H, an appropriate Hilbert space with inner product $(.,.)$ and corresponding norm $\|.\|$. The operator A is a time-invariant differential operator whose domain $D(A)$ is dense in H. A generates a C_0 semigroup $U(t)$ on H which is *dissipative* in the following sense:

$$\|U(t)\| \le M_0 e^{-\sigma_0 t} \qquad (t \ge 0) \tag{2}$$

where $M_0 \ge 1$ and $\sigma_0 > 0$ represents the total natural dissipation in the system. The input operator B has rank M (i.e., M inputs) and the output operator C has rank P (i.e., P outputs); these operators are determined by the type and location of actuators and sensors.

II. Discrete-Time Stability of DVFB: Euler's Method

Suppose that the DVFB control law

$$f = -Qy \tag{3}$$

where $Q > 0$, is used in the distributed parameter system (1) under the assumption of collocated force actuators and velocity sensors, i.e., $C = B^T$. This produces a closed-loop system:

$$v_t = A_c v \tag{4}$$

where $A_c = A - BQB^T$. Under certain conditions on A it is known that the energy is dissipated from Eq. (4); hence, if (A,B) is controllable, Eq. (4) is stable in continuous time. However, the digital implementation of Eq. (3) would sample and hold the sensor outputs over the time interval Δt to produce the discrete-time DVFB control law

$$f(k) = -Qy(k) \tag{5}$$

where $f(k)$ is constant over $(k+1)\Delta t \le t \le k\Delta t$. Consequently, the closed-loop system at each time step behaves in the following way:

$$v(k+1) = \Phi_c v(k) \tag{6}$$

where $\Phi_c = U_c(\Delta t)$ and $U_c(\Delta t)$ is the semigroup generated by A_c evaluated on the time step Δt. Although Eq. (4) is guaranteed to be stable, we want to know how large Δt may become without a loss of stability in the actual system.

We will *assume* for simplicity that dim v is *finite*. However, much of the Lyapunov analysis that is carried out here may be extended to infinite-dimensional systems if one is careful about certain concepts; we leave such extensions for future study.

As a first step, we assume that Euler's method of approximation of the time derivative is used:

$$v_t \approx \frac{v(t+\Delta t) - v(t)}{\Delta t} \tag{7}$$

This is often exactly the approximation used in on-line controller implementation. The Euler approximation causes Eq. (6) to become

$$v(k+1) = v(k) + \Delta t A_c v(k) \tag{8}$$

From the continuous-time analysis of DVFB, it is known that A_c is stable. Therefore, given any positive definite Q, there is a positive definite solution P to the Lyapunov equation

$$PA_c + A_c^T P + Q = 0 \tag{9}$$

For discrete-time stability we consider the Lyapunov function

$$V(v(k)) \equiv \tfrac{1}{2} v^T(k) P v(k)$$

and obtaining

$$\Delta V = -\Delta t [Q - \Delta t A_c^T P A_c] \tag{10}$$

where $\Delta V \equiv V(v(k+1)) - V(v(k))$, we have the following result.

Theorem 1. The discrete-time system Eq. (8) remains stable as long as

$$\Delta t < \frac{\lambda_{\min}(Q)}{\lambda_{\max}(A_c^T P A_c)} \tag{11}$$

Received Jan. 4, 1982.

*Associate Professor. Member AIAA.